Volume 27
Number 20
28 May 2025
Pages 3155–3394

CrystEngComm

rsc.li/crystengcomm

ISSN 1466-8033

ROYAL SOCIETY OF CHEMISTRY

PAPER

Chengzhen Wei *et al.*

Hollow architectures of $CoNi_2S_4/NiS_2$ with boosted performance for supercapacitors

CrystEngComm

ROYAL SOCIETY OF CHEMISTRY

PAPER

View Article Online
View Journal | View Issue

Cite this: *CrystEngComm*, 2025, **27**, 3229

Hollow architectures of $CoNi_2S_4/NiS_2$ with boosted performance for supercapacitors†

Chengzhen Wei, *[abc] Cheng Cheng,[abc] Weichen Lin,[abc] Chenxi Li,[abc] Weimin Du,[abc] Kaige Du[abc] and Shuo Shan[bc]

Received 5th February 2025,
Accepted 6th April 2025

DOI: 10.1039/d5ce00129c

rsc.li/crystengcomm

Hollow architectures have great prospects in supercapacitors due to their rich active surface area, good structural stability and convenient transmission channels for ions/electrons. Herein, we present a self-engaged template process to prepare hybrid $CoNi_2S_4/NiS_2$ hollow architectures. Ni–Co glycerate solid spheres are used as templates and transformed to $CoNi_2S_4/NiS_2$ *via* a sulfidation procedure. The supercapacitor's performance evaluation unveils that these $CoNi_2S_4/NiS_2$ hollow architectures manifest a high capacitance of 1309.2 F g^{-1} at 4.0 A g^{-1} and remarkable cyclability with 1147.6 F g^{-1} retention (only 4.2% decay) for 5000 cycles at 6.0 A g^{-1}. Furthermore, a two-electrode cell assembly of the $CoNi_2S_4/NiS_2$ and activated carbon, displays an energy density of 47.5 W h kg^{-1} at 3301 W kg^{-1} and impressively durable cycle life. These results provide a simple avenue to design an efficient electrode material for supercapacitors based on metal sulfides.

1. Introduction

Supercapacitors with long cycle lives, ideally large power density and high reliability, have received intense research interest in recent years.[1] Exploring potential electrode materials is crucial to achieve the desirable performance of supercapacitors.[2] To date, many explorations have been made to obtain suitable electrode materials for supercapacitors. Among the various alternatives, transition metal sulfides are deemed to be promising candidates due to their abundant active sites, significant capacity and efficient electric conductivity.[3–5] In comparison with single metal sulfides, construction of different metal sulfides into one advanced architecture is valid for promoting the electrochemical features with boosted conductivity, electroactivity and structural stability, owing to the synergetic effects of each metal sulfide.[6–8] For instance, $Ni_3S_2@Co_3S_4$ composites were designed to exhibit high specific capacitance, exceptional rate capacity and cycling behavior for supercapacitors.[9] A $Co_9S_8@Ni_3S_2/ZnS$ composite formed *via* a template assisted method has been reported; the unique composite and architecture endow $Co_9S_8@Ni_3S_2/ZnS$ with remarkable electrochemical properties.[10] As a result, exploring metal sulfides with complex components is highly significant for high performance supercapacitors.

Many facts have affirmed that electrode materials with tunable architectures have a significant effect on supercapacitor performance.[11,12] In this context, an effective way is to fabricate desirable electrode material architectures for high performance. Hollow architectures possess attractive features of rich inner space, a short ion permeation channel, large surface area and incremental electrolyte–electrode contact area.[13–15] For example, a hollow $NiCo_2S_4/Co_9S_8$ spindle electrode material that shows high pseudocapacitance and energy density has been reported.[16] Zhao *et al.* explored a NiS_2/CuS hollow microsphere that manifested outstanding pseudocapacitive as well as exceptional cycling life and rate behavior.[17] Therefore, hollow architectures are considered as versatile electrode materials for electrochemical energy storage.

Ni–Co sulfides have higher conductivity and richer redox reactions and are promising candidates for supercapacitor electrode materials. In particular, $CoNi_2S_4$ is an outer layer material,[18] which exhibits high conductivity and can boost electron transport and initiate ionic reactions. Moreover, NiS_2, featuring large theoretical capacity is another promising candidate for supercapacitors. Therefore, some beneficial $CoNi_2S_4$ or NiS_2 supercapacitor electrode materials have been reported. However, hybrid $CoNi_2S_4/NiS_2$ hollow architectures are rarely reported. Herein, we exploit a self-engaged template method to prepare hybrid $CoNi_2S_4/NiS_2$ hollow

[a] *Henan Province Key Laboratory of New Opto-electronic Functional Materials, College of Chemistry and Chemical Engineering, Anyang Normal University, Anyang 455000, P. R. China. E-mail: chengzhenweichem@126.com*
[b] *Henan Province Engineering and Technology Research Center for Aqueous System Energy Storage and Conversion Electrode Materials, China*
[c] *Henan Province Engineering Research Center of Chemical Energy-saving Material Development and Application, China*

† Electronic supplementary information (ESI) available. See DOI: https://doi.org/10.1039/d5ce00129c

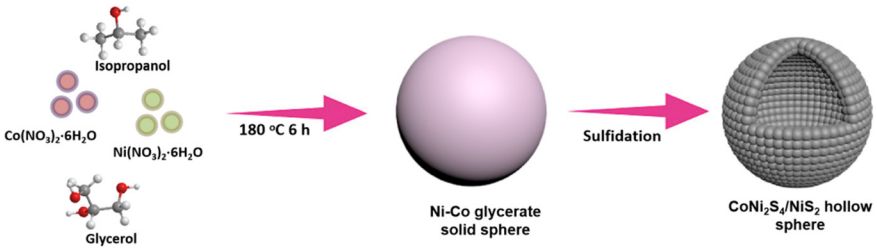

Scheme 1 Schematic synthesis procedure toward $CoNi_2S_4/NiS_2$ hollow architectures.

architectures, as shown in Scheme 1. As a result of the architecture and components, the $CoNi_2S_4/NiS_2$ demonstrates remarkable performance, delivering a high capacitance of 1309.2 F g^{-1} at 4.0 A g^{-1} and excellent durability with 1147.6 F g^{-1} retention (only 4.2% loss) over 5000 cycles at 6.0 A g^{-1}. Moreover, the constructed two-electrode device with $CoNi_2S_4/NiS_2$ and activated carbon (AC) shows a high energy density of 47.5 W h kg^{-1} at 3301 W kg^{-1} and superb cycle life. These results suggest its great potential for electrochemical energy storage.

2. Experimental

2.1 Preparation of Ni–Co glycerate precursor

In a typical precursor preparation, $Ni(NO_3)_2·6H_2O$ (0.40 mmol) and $Co(NO_3)_2·6H_2O$ (0.10 mmol) are solubilized in a

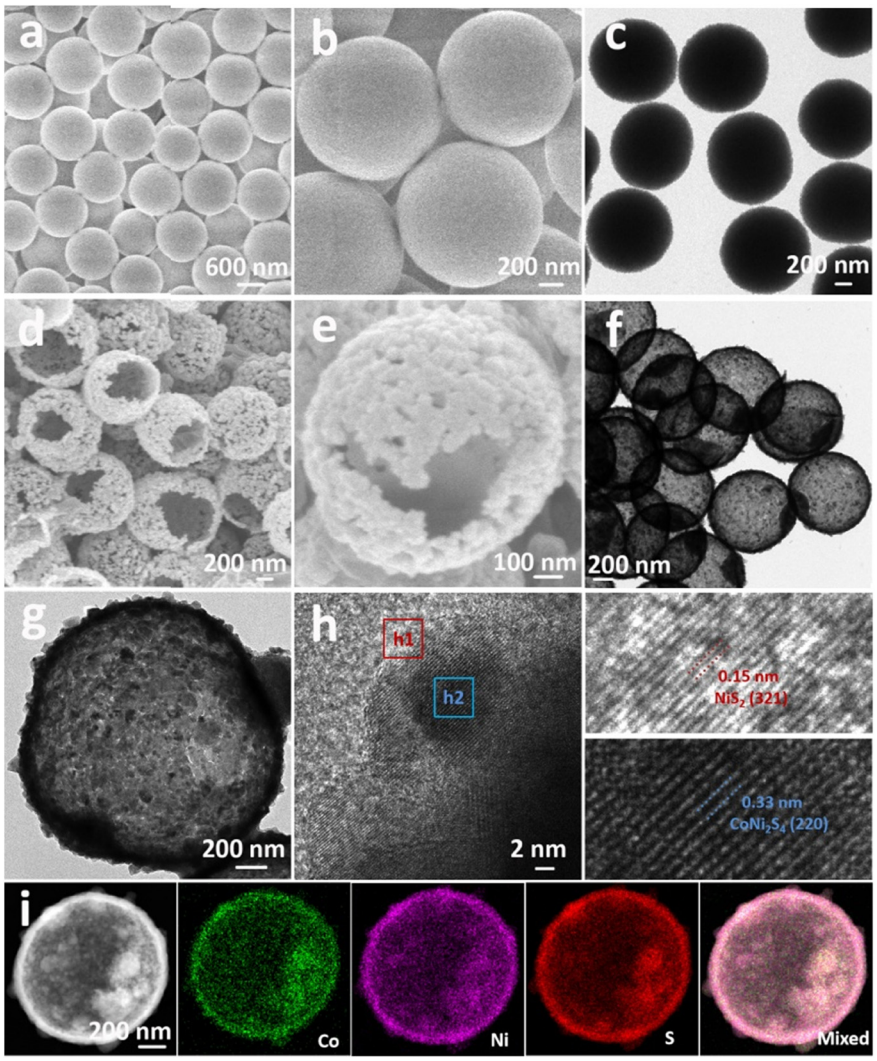

Fig. 1 (a and b) FESEM and (c) TEM images of Ni–Co glycerate, (d and e) FESEM and (f and g) TEM images of $CoNi_2S_4/NiS_2$ hollow architectures, (h and i) HRTEM and TEM elemental mapping images of $CoNi_2S_4/NiS_2$ hollow architectures.

mixture of 8.0 mL glycerol and 40 mL isopropanol under stirring. Then the solution is placed into an autoclave and heated at 180 °C for 6.0 h. Finally, the resulting solution is centrifuged, purified with ethanol and dried, providing the precursor of the Ni–Co glycerate.

2.2 Synthesis of $CoNi_2S_4/NiS_2$ hollow architectures

Typically, 30 mg precursor is dispersed in 20 mL ethanol under stirring. Then 50 mg thioacetamide (TAA) is added into the dispersion and further stirred for about 30 min. The solution is sealed in an autoclave and heated at 160 °C for 6.0 h. After centrifugation, purification with ethanol and drying, the Ni–Co sulfide product is obtained.

2.3 Sample characterization

The architecture observation was performed using a scanning electron microscope (SEM; Hitachi, SU8010) and transmission electron microscope (TEM; Tecnai, G2F30). To acquire the sample composition, X-ray diffraction (XRD) patterns were obtained using a Rigaku D/max 2500 diffractometer. The chemical states of each element in the Ni–Co sulfide were characterized using an X-ray photoelectron spectrometer (XPS; Thermo, Escalab250Xi). Nitrogen adsorption–desorption characterization was conducted using an ASAP 2020 Micromeritics instrument.

2.4 Electrochemical tests

Electrochemical tests were performed on a CHI 660D electrochemical workstation using a three-electrode system in 3.0 M KOH electrolyte, in which Hg/HgO/sat. KCl electrode and platinum foil acted as the reference electrode and counter electrode. The Ni–Co sulfide, acetylene black and polyvinylidene difluoride (mass ratio = 85 : 10 : 5) were polished in isopropanol for about 30 min and further dropped on a nickel foam as the working electrode. The mass loading of the $CoNi_2S_4/NiS_2$ hollow architectures electrode material for the three electrode system is about 5 mg.

The asymmetric supercapacitor tests were measured in 3.0 M KOH electrolyte with a two-electrode system: an AC negative electrode and Ni–Co sulfide positive electrode. AC, acetylene black and polyvinylidene difluoride (mass ratio = 85 : 10 : 5) were added in isopropanol. After grinding the mixture for 30 min, the resultant slurry was coated on a nickel foam to provide the negative electrode. Similarly, the fabrication of the positive electrode resembles the process for the negative electrode except the AC was replaced by the Ni–Co sulfide. The mass ratio between $CoNi_2S_4/NiS_2$ and AC was around 1 : 2. The energy density (E) and power density (P) of the asymmetric supercapacitor can be calculated, as shown in eqn (1) and (2),

$$E = \frac{C \times (\Delta V)^2}{7.2} \left(\mathrm{W\ h\ kg^{-1}}\right) \quad (1)$$

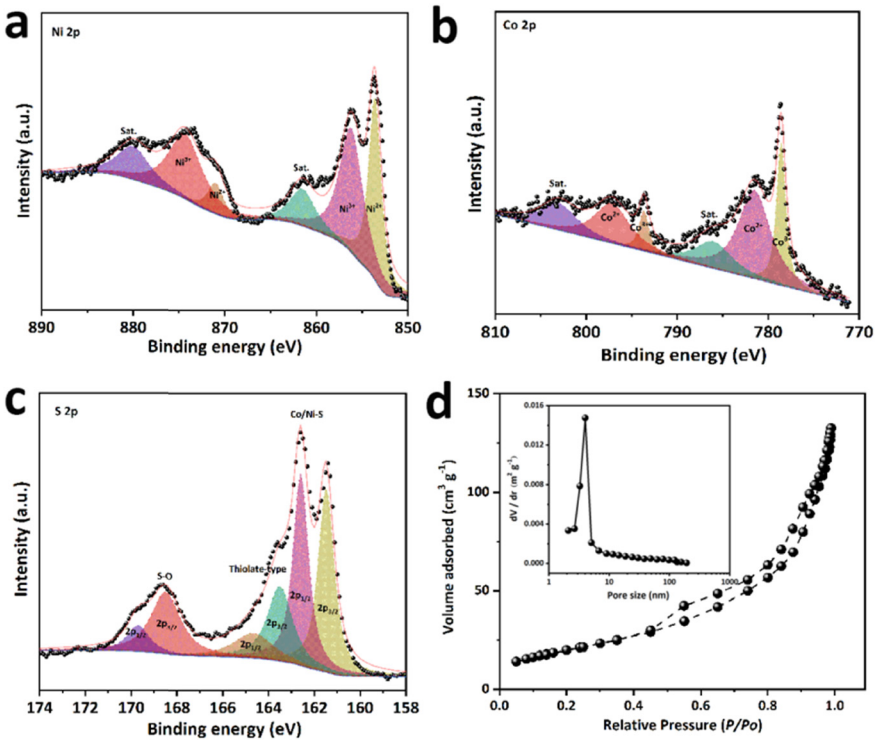

Fig. 2 (a) Ni 2p, (b) Co 2p and (c) S 2p XPS spectra of the $CoNi_2S_4/NiS_2$ hollow architectures; (d) N_2 adsorption/desorption isotherms and the corresponding pore size distributions (inset) of the $CoNi_2S_4/NiS_2$ hollow architectures.

$$P = \frac{3600E}{\Delta t}\,(\mathrm{W\ kg^{-1}}) \quad (2)$$

where C (F g^{-1}) and ΔV (V) stand for the specific capacitance and working voltage, Δt (s) denotes discharging process time.

3. Results and discussion

As analyzed by FESEM and TEM (Fig. 1a–c), the Ni–Co glycerate forms solid spheres with a diameter of about 1.0 μm and smooth surfaces. The obtained Ni–Co glycerate is subsequently sulfurized by reacting with TAA under solvothermal conditions. Eventually, the Ni–Co sulfide is synthesized. The hollow architectures can be distinctly observed for the Ni–Co sulfide. A careful observation of the shell of the Ni–Co sulfide, we see that the hollow architecture is constructed by nanoparticles (Fig. 1d–g). To illustrate the hollow architecture formation process, samples prepared at various time intervals were observed by TEM, as shown in Fig. S1.† The samples still form solid spheres but possess a rough surface after 0.5 h (Fig. S1a†), demonstrating the occurrence of sulfidation reactions on the Ni–Co glycerate precursor surface. After 1.0 h, a core–shell structured is formed (Fig. S1b†). Extending the sulfidation time to 3.0 h, the core becomes smaller (Fig. S1c†). Further increasing the sulfidation time to 6 h, the core is consumed completely, and the hollow architecture is finally formed (Fig. 1f and g).The XRD result (Fig. S2†) proves that the derived Ni–Co sulfide includes $CoNi_2S_4$ (JCPDS No. 24-0334) and NiS_2 (JCPDS No. 11-0099). A high resolution TEM (HRTEM) image shows lattice distances of 0.15 nm and 0.33 nm (Fig. 1h), which conform to the (321) plane of NiS_2 and (220) plane of $CoNi_2S_4$, respectively. As shown in the elemental mapping images of a Ni–Co sulfide (Fig. 1i), the Co, Ni and S elements are evenly distributed in the hollow architecture. Moreover, the electronic states of Ni, Co and S elements in the $CoNi_2S_4/NiS_2$ were further characterized using XPS. In the Ni 2p spectra (Fig. 2a), peaks at 853.5 and 871 eV are associated with Ni^{2+} Ni $2p_{3/2}$ and $2p_{1/2}$,[19] while peaks emerging at 856.3 and 874.4 eV, are attributed to the Ni^{3+} Ni $2p_{3/2}$ and $2p_{1/2}$.[20] The Co 2p spectra (Fig. 2b) shows pronounced peaks at 778.6 and 793.6 eV, which ascribe to Co^{3+} Co $2p_{3/2}$ and $2p_{1/2}$.[21] Another two

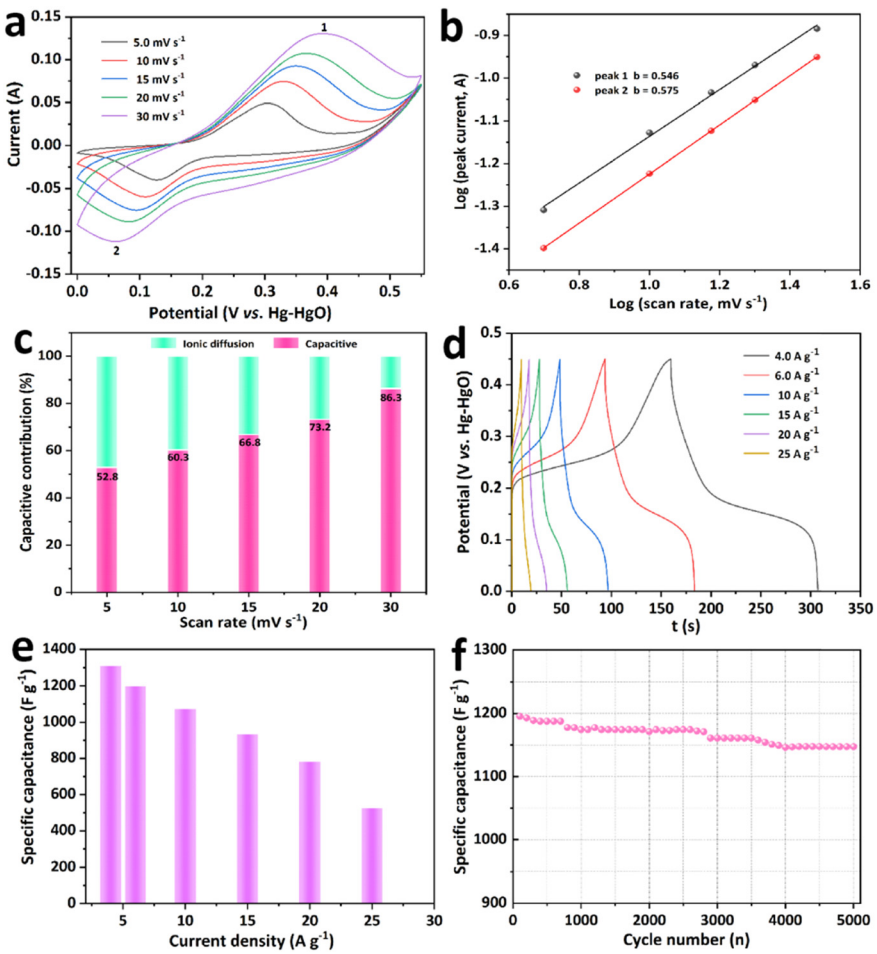

Fig. 3 Electrochemical behavior of the $CoNi_2S_4/NiS_2$ hollow architectures as supercapacitors: (a) CV curves at scanning rates of 5.0 to 30 mV s^{-1}; (b) the linear relationships between log (peak currents) and log (scanning rates); (c) capacitive contribution ratios at various scanning rates; (d) GCD; and specific capacitance profiles (e) at various current densities; (f) continuous cycling performance at 6.0 A g^{-1} after 5000 cycles.

peaks at 781.5 and 797.3 eV are assigned to Co^{2+} Co $2p_{3/2}$ and $2p_{1/2}$.[22] The S 2p spectra of the Ni–Co glycerate derivative presents the peaks at 162.6 and 168.5 eV, which are correlated with Co/Ni–S and S–O bonds (Fig. 2c).[23] These above analyses confirm the successful preparation of the $CoNi_2S_4/NiS_2$ hollow architecture.

Due to the special structural characteristics, a large surface area of 75.4 m^2 g^{-1} with mesoporous structure for Ni–Co sulfide hollow architectures illustrates the existence of considerable active sites that can boost the electrochemical performance (Fig. 2d). The supercapacitor behavior of the Ni–Co sulfide electrode material is firstly studied in the three-electrode cell. Fig. 3a shows the cyclic voltammetry (CV) curves of the Ni–Co sulfide electrode measured at a scan rate of 5.0–30 mV s^{-1}. The distinct redox peaks can be discerned, revealing the Faradaic features of the Ni–Co sulfide. The capacitive effect analysis is further evaluated using eqn (3):[24]

$$i = av^b \quad (3)$$

where i corresponds to the current response at oxidation/reduction peaks and v represents the scan rate, while a and b stand for the experimental parameters. The parameter b is 0.5, signifying that ionic diffusion is dominant. A b value of 1.0 denotes the electrochemical reaction is mainly due to capacitive behavior. As shown in Fig. 3b, b values of 0.546 and 0.575 for Ni–Co sulfide suggest the charging process is governed by both ionic diffusion and capacitive behavior. The Faradaic redox process could be expressed using the following equations:[18,25]

$$CoNi_2S_4 + OH^- + H_2O \rightleftharpoons CoSOH + 2NiSOH + e^- \quad (4)$$

$$CoSOH + OH^- \rightleftharpoons CoSO + H_2O + e^- \quad (5)$$

$$NiSOH + OH^- \rightleftharpoons NiSO + H_2O + e^- \quad (6)$$

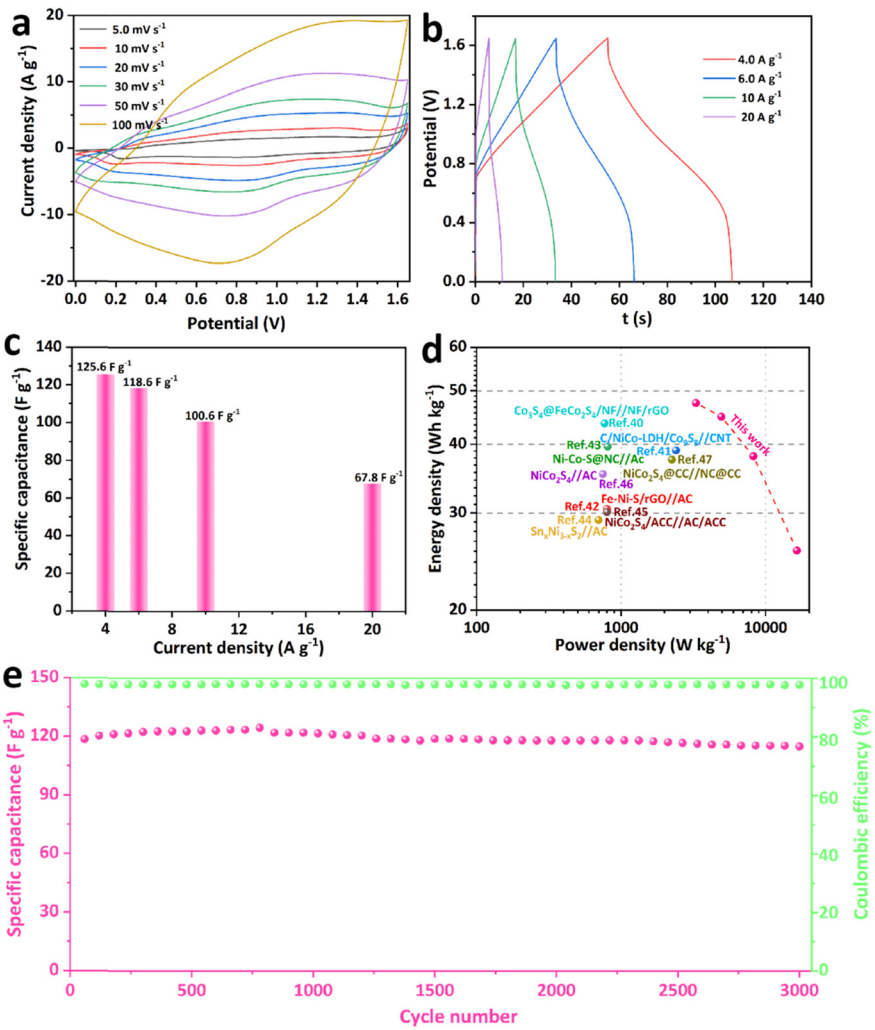

Fig. 4 Electrochemical performance of the two-electrode system: (a) CV profiles at scanning rates of 5.0 to 100 mV s^{-1}; (b) GCD profiles in current densities of 4.0 to 20 A g^{-1}; (c) specific capacitance at various current densities; (d) Ragone plots; and (e) cycling stability for 3000 cycles at 6.0 A g^{-1}.

$$NiS_2 + OH^- \rightleftharpoons NiS_2OH + e^- \quad (7)$$

To further quantitatively analyse the contribution fraction of ionic diffusion and capacitive behavior , the following eqn (8) is applied:

$$i(V) = k_1v + k_2v^{1/2} \quad (8)$$

where $i(V)$ is the response current *versus* operating voltage of V, k_1v and $k_2v^{1/2}$ represent the capacitive and ionic diffusion in the redox processes, with k_1 and k_2 acquired from the relationship $i(V)/v^{1/2}$ *versus* $v^{1/2}$.[26] As illustrated in Fig. 3c and Fig. S3,† a 52.8% capacitive contribution for Ni–Co sulfide is obtained at 5.0 mV s^{-1}, and the capacitive contribution increases from 60.3 to 86.3 as the scan rate varies from 10 to 30 mV s^{-1}.

Representative galvanostatic charge/discharge (GCD) profiles of the Ni–Co sulfide at current densities from 4.0 to 25 A g^{-1} are displayed in Fig. 3d. Also, Ni–Co sulfide electrode shows charge/discharge platforms, further indicating the Faradaic behavior of the material,[27] which is in accordance with the CV characterizations. As shown in Fig. 3e, the Ni–Co sulfide electrode acquires a high capacitance of 1309.2 F g^{-1} at 4.0 A g^{-1}. At 25 A g^{-1}, a capacitance of 525 F g^{-1} still remains. Certainly, results of cycling measurements uncover that the Ni–Co sulfide exhibits remarkable electrochemical stability (Fig. 3f), and 1147.6 F g^{-1} is retained after 5000 cycles at 6.0 A g^{-1}. The decay of electrochemical stability after cycling can be ascribed to the hollow architecture volume variation associated with repeated charge/discharge. The impedance plots of the $CoNi_2S_4/NiS_2$ hollow architectures are shown in Fig. S4.† The R_s values for before and after 5000 cycles are determined to be 0.17 and 0.55 Ω, confirming that the R_s changed slightly after the cycles. Moreover, there is not much change in the CV and GCD curves after the cycles (Fig. S5†). Of note, the $CoNi_2S_4/NiS_2$ electrode with hollow architecture structure is preserved after continuous cycles (Fig. S6†), demonstrating the stability of the $CoNi_2S_4/NiS_2$ hollow architectures electrode material for long term cycling. So it is assumed that the desired cycling of $CoNi_2S_4/NiS_2$ is attributed to the unique hollow architectures that store electrolytes and shorten ion diffusion routes, and enhance the conductivity and optimize electron transfer of the material. Also, compared with previously reported hybrid metal sulfide electrodes for supercapacitors, the Ni–Co sulfide hollow architectures show comparable or obvious superiority (Table 1).[13,28–37]

To delve into its practical application, we assembled a two-electrode configuration in which 3.0 M KOH, Ni–Co sulfide and AC served as the electrolyte, positive and negative electrodes, respectively. The CV profiles were performed at different scan rates from 0 to 1.6 V. As is noticeably displayed in Fig. 4a, the profiles feature an asymmetrical rectangle-like shape with broad and weak redox peaks, confirming that the device has double layer capacitive and pseudocapacitive peculiarities. Moreover, the original shape of the CV profiles is retained at scan rates from 5 to 100 mV s^{-1}, unveiling the remarkable rate capabilities.[38] The GCD profiles (Fig. 4b) are virtually symmetric in the current densities of 4.0 to 20 A g^{-1}, which implies its excellent electrochemical reversibility.[39] Fig. 4c reveals that the device achieves 125.6, 118.6, 100.6 and 67.8 F g^{-1} from 4.0 to 20 A g^{-1}. The determined Ragone plots show that the energy density of the device is 47.5 W h kg^{-1} at 3301 W kg^{-1}, and reaches 26 W h kg^{-1} at 16481 W kg^{-1} (Fig. 4d), which is better than reported asymmetric supercapacitor devices, such as Co_3S_4@$FeCo_2S_4$/NF//NF/rGO (43.6 W h kg^{-1} at 770 W kg^{-1}),[40] C/NiCo-LDH/Co_9S_8//CNT (39.0 W h kg^{-1} at 2400 W kg^{-1}),[41] Fe–Ni–S/rGO//AC (30.5 W h kg^{-1} at 800 W kg^{-1}),[42] Ni–Co–S@NC//AC (43.6 W h kg^{-1} at 770 W kg^{-1}),[43] $Sn_xNi_{3-x}S_2$//AC (29.13 W h kg^{-1} at 700 W kg^{-1}),[44] $NiCo_2S_4$/ACC//AC/ACC (30.1 W h kg^{-1} at 800.2 W kg^{-1}),[45] $NiCo_2S_4$//AC (35.3 W h kg^{-1} at 750 W kg^{-1}),[46] and $NiCo_2S_4$@CC//NC@CC (37.5 W h kg^{-1} at 2250 W kg^{-1}).[47] Remarkably, as shown in Fig. 4e, the device retains its performance over 3000 charge/discharge cycles with about a 3.0% decline, under 6.0 A g^{-1}. Moreover, the device can retain a Coulombic efficiency of ~99.6% during the cycles, suggesting its remarkable reversibility. Above all, these results show that the developed hybrid $CoNi_2S_4/NiS_2$ hollow architecture has very promising application potential in energy storage.

The remarkable capacitive behaviors can be accounted for by the following advantages. First, the hollow architectures with structural stability not only endow considerable electroactive sites but also provide convenient transmission channels for ions/electrons, which generate the high capacitance and excellent cyclability. Second, the synergistic effect combining the advantages of $CoNi_2S_4$ and NiS_2 renders the hybrid $CoNi_2S_4/NiS_2$ with the desired electrochemical performance. In short, profiting from its architecture and the properties of its component parts, the hollow architecture of $CoNi_2S_4/NiS_2$ is deemed to be an ideal candidate for supercapacitor materials.

4. Conclusions

In summary, hybrid $CoNi_2S_4/NiS_2$ hollow architectures are developed as a potentially excellent supercapacitor material. The $CoNi_2S_4/NiS_2$ is obtained *via* a self-engaged template route to synthesize Ni–Co glycerate, followed by a sulfidation procedure. Profiting from the hollow architectures and complex components, the $CoNi_2S_4/NiS_2$ shows a high capacitance of 1309.2 F g^{-1} at 4.0 A g^{-1}, and remarkable durability with 1147.6 F g^{-1} maintained over 5000 cycles under 6.0 A g^{-1}. Furthermore, a two-electrode configuration with the $CoNi_2S_4/NiS_2$ and AC achieves a high energy density of 47.5 W h kg^{-1} at 3301 W kg^{-1} and excellent cycle life. This work would offer a valid avenue to design high performance supercapacitor materials.

Table 1 Comparison of the electrochemical performance of the $CoNi_2S_4/NiS_2$ hollow architectures with previously reported counterparts

Electrode materials	Morphology	Current density	Specific capacitance	Capacitance retention	Reference
Mo-doped CoS hollow nanocages		0.5 A g^{-1}	781 F g^{-1}	46.8% after 5000 cycles	28
Hollow dodecahedral $Co_4S_3/MoS_2/MnS$		1.0 A g^{-1}	590 F g^{-1}	90% after 45 000 cycles	29
Hollow MnS@MoS_2 cubes		1.0 A g^{-1}	1713.4 F g^{-1}	96.8% after 1000 cycles	30
Hollow $CuCo_2S_4$ cages		0.5 A g^{-1}	1096.27 F g^{-1}	—	13
Hollow urchin-like $CuCo_2S_4$		1.0 A g^{-1}	1069 F g^{-1}	93.7% after 10 000 cycles	31
Hollow $NiCo_2S_4$ ellipsoids		10 A g^{-1}	495 F g^{-1}	—	32
Carbon coated $NiCo_2S_4$ hollow spheres		1.0 A g^{-1}	935 F g^{-1}	103.1% after 25 000 cycles	33
Hollow core–shell $NiCo_2S_4$@MoS_2		1.0 A g^{-1}	860 F g^{-1}	71.9% after 1000 cycles	34
Rod-shaped $CoNi_2S_4$		2.0 mA cm^{-2}	7.54 F cm^{-2}	71.25% after 5000 cycles	35
Yolk–shell $(NiCo)_9S_8$/GC spheres		1.0 A g^{-1}	1367 F g^{-1}	89.2% after 6000 cycles	36
Double-shelled hollow $MnCo_2S_4/CoS_{1.097}$ spheres		1.0 A g^{-1}	1006 F g^{-1}	91.3% after 5000 cycles	37
Hollow $CoNi_2S_4/NiS_2$ hollow spheres		**4.0 A g^{-1}**	**1309.2 F g^{-1}**	**95.9% after 5000 cycles**	**This work**

Data availability

The authors confirm that the data supporting the findings of this study are available within the article and its ESI.†

Conflicts of interest

There are no conflicts to declare.

Acknowledgements

This work was financed by the Major Science and Technology Special Project of Anyang City (2023A02GX009).

Notes and references

1 A. L. Narayana, N. Attarzadeh, V. Shutthanandan and C. V. Ramana, High-performance $NiCo_2O_4$/Graphene quantum dots for asymmetric and symmetric supercapacitors with enhanced energy efficiency, *Adv. Funct. Mater.*, 2024, **34**, 2316379.

2 Q. H. Wu, T. Q. He, Y. K. Zhang, J. L. Zhang, Z. J. Wang, Y. Liu, L. Zhao, Y. Z. Wu and F. Ran, Cyclic stability of supercapacitors: materials, energy storage mechanism, test methods, and device, *J. Mater. Chem. A*, 2021, **9**, 24094–24147.

3 R. Tian, Y. Zhou, H. N. Duan, Y. P. Guo, H. Li, K. F. Chen, D. F. Xue and H. Z. Liu, MOF-derived hollow Co_3S_4 quasi-polyhedron/MWCNT nanocomposites as electrodes for advanced lithium ion batteries and supercapacitors, *ACS Appl. Energy Mater.*, 2018, **1**, 402–410.

4 H. T. Niu, Y. Liu, B. D. Mao, N. Xin, H. Jia and W. D. Shi, In-situ embedding MOFs-derived copper sulfide polyhedrons in carbon nanotube networks for hybrid supercapacitor with superior energy density, *Electrochim. Acta*, 2020, **329**, 135130.

5 M. Y. Zhu, X. Li, C. Y. Tu, Q. Luo, Y. J. Nie, J. M. Pan and S. J. Li, Ethylene glycol assisted self-template conversion approach to synthesize hollow NiS microspheres for a high performance all-solid-state supercapacitor, *Mater. Chem. Front.*, 2022, **6**, 203–212.

6 C. P. Yu, Y. Li, Y. Wang, J. W. Cui, T. Y. Zhu, D. B. Yu, X. Shu, Y. Zhang, D. R. MacFarlane and Y. C. Wu, Enhanced energy storage performance of 3D hybrid metal sulfides via synergistic engineering of architecture and composition, *ACS Sustainable Chem. Eng.*, 2020, **8**, 11491–11500.

7 Y. Wang, X. S. Wang, X. J. Dai, K. L. Li, Z. H. Bao, H. Y. Li, H. W. Tian, P. A. Yang, H. Zhou, H. Chen, Y. L. Yu, P. Yan and Y. X. Zhang, Structural evolution and sulfuration of nickel cobalt hydroxides from 2D to 1D on 3D diatomite for supercapacitors, *CrystEngComm*, 2021, **23**, 5636–5644.

8 J. C. Qi, H. Y. Duan, Z. L. Peng, J. Wang, B. X. Ma, Z. H. Yuan and H. F. Zhang, Cobalt-nickel mixed sulfide hollow nanocages with enhanced surface induced capacitive storage for hybrid supercapacitor, *Energy Fuels*, 2024, **38**, 13379–13389.

9 Q. Zhang, Q. S. Shi, Y. Yang, Q. Zhang, Z. Y. Xiao, X. H. Zhang and L. Wang, 2D nanosheet/3D cubic framework Ni–Co sulfides for improved supercapacitor performance via structural engineering, *Dalton Trans.*, 2020, **49**, 8162–8168.

10 H. M. Chen, J. J. Zhou, Q. Li, S. H. Zhao, X. B. Yu, K. Tao, Y. P. Hu and L. Han, MOF-assisted construction of a Co_9S_8@Ni_3S_2/ZnS microplate array with ultrahigh areal specific capacity for advanced supercapattery, *Dalton Trans.*, 2020, **49**, 10535–10544.

11 X. T. Mei, C. Yang, F. Y. Chen, Y. T. Wang, Y. Zhang, Z. M. Man, W. Y. Lu, J. H. Xu and G. Wu, Interfacially ordered NiCoMoS nanosheets arrays on hierarchical $Ti_3C_2T_x$ Mxene for high-energy-density fiber-shaped supercapacitors with accelerated pseudocapacitive kinetics, *Angew. Chem., Int. Ed.*, 2024, **63**, e202409281.

12 X. Cui, F. W. Ma, G. P. Lei, W. Jiang, X. Y. Yang, Z. Y. Liu, J. F. Wan and Y. F. Liu, Trisodium citrate as a double-edged sword: selective etching Prussian blue analog nanocubes into orthogonal frustums and their derivatives for supercapacitors, *Small*, 2024, **20**, 2403732.

13 J. Q. Wang, Y. L. Quan, G. X. Wang, D. Z. Wang, J. Xiao, S. P. Gao, H. F. Xu, S. Liu and L. Cui, 3D hollow cage copper cobalt sulfide derived from metal-organic frameworks for high-performance asymmetric supercapacitors, *CrystEngComm*, 2021, **23**, 7385–7396.

14 Y. X. Zeng, Z. H. Pei, D. Y. Luan and X. W. David Lou, Atomically dispersed zincophilic sites in N, P-codoped carbon macroporous fibers enable efficient Zn metal anodes, *J. Am. Chem. Soc.*, 2023, **145**, 12333–12341.

15 H. Tong, L. Li, C. Q. Wu, Z. Tao, J. H. Fang, C. Y. Guan and X. G. Zhang, Sea urchin-like NiCo-LDH hollow spheres anchored on 3D graphene aerogel for high-performance supercapacitors, *ChemSusChem*, 2024, **17**, e202400142.

16 L. R. Hou, Y. Y. Shi, S. Q. Zhu, M. Rehan, G. Pang, X. G. Zhang and C. Z. Yuan, Hollow mesoporous hetero-$NiCo_2S_4$/Co_9S_8 submicro-spindles: unusual formation and excellent pseudocapacitance towards hybrid supercapacitors, *J. Mater. Chem. A*, 2017, **5**, 133–144.

17 W. X. Zhao, X. D. Wang, X. Q. Ma, L. C. Yue, Q. Liu, Y. L. Luo, Y. Liu, A. M. Asiri and X. P. Sun, *In situ* tailoring bimetallic-organic framework-derived yolk-shell NiS_2/CuS hollow microspheres: an extraordinary kinetically pseudocapacitive nanoreactor for an effective sodium-ion storage anode, *J. Mater. Chem. A*, 2021, **9**, 15807–15819.

18 J. J. Hu, L. Sun, F. Xie, Y. R. Qu, H. K. Tan, X. C. Shi, J. L. Qian, K. Wang and Y. H. Zhang, A sandwich-like CoNiLDH@rGO@$CoNi_2S_4$ electrode enabling high mass loading and high areal capacitance for solid-state supercapacitors, *J. Mater. Chem. A*, 2022, **10**, 21590–21602.

19 H. Z. Wang, X. Gao, Y. Q. Xie, E. J. Guo, H. Bai, F. Jiang, Q. Li and H. Y. Yue, Design and fabrication of island-like $CoNi_2S_4$@NiCo-LDH/biomass carbon heterostructure as advanced electrodes for high-performance hybrid supercapacitors, *Adv. Energy Mater.*, 2024, **14**, 2400493.

20 Q. Hu, Y. C. Bai, Y. L. Fang, L. Guo and W. P. Li, Acid- and alkaline-induced phase and structure reconstruction of nickel sulfide toward enhanced electrochemical performance, *CrystEngComm*, 2024, **26**, 5393–5404.

21 X. F. Lu, S. L. Zhang, W. L. Sim, S. Y. Gao and X. W. David Lou, Phosphorized $CoNi_2S_4$ yolk-shell spheres for highly efficient hydrogen production via water and urea electrolysis, *Angew. Chem., Int. Ed.*, 2021, **60**, 22885–22891.

22 C. L. Lv, J. H. Wei, F. Hu, L. M. Bian and Q. Y. Ouyang, Effect of sulfur vacancies of $CoNi_2S_4$ on its electrochemical performance in hybrid supercapacitors, *Langmuir*, 2024, **40**, 27386–27395.

23 Z. Wang, J. Jian, X. Y. Wang, Y. Qiao, M. T. Wang, S. Gao, P. Nie and L. M. Chang, $CoNi_2S_4$@CoNi-LDH heterojunction grown on SSM as a highly efficient trifunctional catalyst for water splitting and Zn-air batteries, *J. Mater. Chem. C*, 2023, **11**, 16384–16389.

24 J. J. Ban, X. H. Wen, H. H. Lei, G. Q. Cao, X. H. Liu, C. Y. Niu, G. S. Shao and J. H. Hu, In-plane grain boundary induced defect state in hierarchical NiCo-LDH and effect on battery-type charge storage, *Nano Res.*, 2023, **16**, 4908–4916.

25 J. J. Hu, L. Sun, F. Xie, Y. R. Qu, H. K. Tan and Y. H. Zhang, An urchin-like Co-doped NiS_2/C nanorod array with enriched sulfur vacancies for asymmetric supercapacitors, *J. Mater. Chem. A*, 2023, **11**, 8380–8391.

26 G. B. Bhanuse, S. Kumar, C. C. Yu and Y. P. Fu, Nanostructured $ZnCo_2O_4$@NiMn-LDH electrodes for supercapacitor and zinc-air battery application, *ACS Appl. Nano Mater.*, 2024, **7**, 13649–13663.

27 H. L. Jiang, Q. Ke, X. H. Qiu, J. Z. Chen, P. H. Chen, S. Wang, X. B. Luo and B. Y. Rao, NiCo layered double hydroxide nanocages for high performance asymmetric supercapacitors, *Inorg. Chem. Front.*, 2023, **10**, 2154–2164.

28 Z. Yang, Q. X. Ma, L. Han and K. Tao, Design of Mo-doped cobalt sulfide hollow nanocages from zeolitic imidazolate frameworks as advanced electrodes for supercapacitors, *Inorg. Chem. Front.*, 2019, **6**, 2178–2184.

29 X. H. Wang, G. H. Ren, B. N. Chen, J. Liu, X. X. Lv, A. Li, Y. J. Han, J. G. Tao, J. H. Dong and D. Nan, Built-in electric field enhanced electrochemical performance of metal-organic frameworks (MOFs)-derived hollow dodecahedral Co_4S_3/MoS_2/MnS heterostructures, *J. Phys. Chem. C*, 2024, **128**, 15829–15842.

30 Q. N. Zhou, W. Li, H. Z. Xu, M. Y. Gao, X. C. Dong and J. J. Lin, Fabrication of hierarchical integrated 3D hollow MnS@MoS_2 microcubes *via* a template-controlled synthesis for asymmetric supercapacitors, *J. Mater. Chem. A*, 2022, **10**, 9370–9379.

31 H. N. Jia, Y. F. Cai, Z. Y. Wang, X. H. Zheng, C. Li, H. Y. Liang, J. L. Qi, J. Cao, J. C. Feng and W. D. Fei, Sea urchin-like $CuCo_2S_4$ microspheres with a controllable interior structure as advanced electrode materials for high-performance supercapacitors, *Inorg. Chem. Front.*, 2020, **7**, 603–609.

32 L. R. Hou, R. Q. Bao, Z. Y. Chen, M. Rehan, L. N. Tong, G. Pang and C. Z. Yuan, Comparative investigation of hollow mesoporous $NiCo_2S_4$ ellipsoids with enhanced pseudo-capacitances towards high-performance asymmetric supercapacitors, *Electrochim. Acta*, 2016, **214**, 76–84.

33 Z. B. Wang, Y. H. Hao, W. J. Zhang, J. Y. Fang and C. N. Chen, Facile fabrication of carbon-coated spinel nickel-cobalt-sulfide hollow spheres to achieve high-performance supercapacitors, *New J. Chem.*, 2021, **45**, 12150–12158.

34 X. Z. Song, F. F. Sun, Y. L. Meng, Z. W. Wang, Q. F. Su and Z. Q. Tan, Hollow core-shell $NiCo_2S_4$@MoS_2 dodecahedrons with enhanced performance for supercapacitors and hydrogen evolution reaction, *New J. Chem.*, 2019, **43**, 3601–3608.

35 Q. H. Chen, W. N. Zhao, Z. H. Huang, G. C. Li, K. Tao and L. Han, Controlled preparation of $CoNi_2S_4$ nanorods derived from MOF-74 nanoarrays involving an exchange reaction for high energy density supercapacitors, *Dalton Trans.*, 2023, **52**, 9346–9355.

36 Y. L. Liu, C. Yan, G. G. Wang, F. Li, Y. Shang, H. Y. Zhang, J. C. Han and H. Y. Yang, Self-templated formation of $(NiCo)_9S_8$ yolk-shelled spheres for high-performance hybrid supercapacitors, *Nanoscale*, 2020, **12**, 23497–23505.

37 X. Yu, J. L. Yu, L. Hou, A. Gagnoud, Y. Fautrelle, Z. M. Ren and X. Li, Double-shelled hollow hetero-$MnCo_2S_4$/$CoS_{1.097}$ spheres with carbon coating for advanced supercapacitors, *J. Power Sources*, 2018, **408**, 65–73.

38 G. R. Reddy, B. Sravani, N. Jung, G. R. Dillip and S. W. Joo, Engineering rich-cation vacancies in $CuCo_2O_4$ hollow spheres with a large surface area derived from a template-free approach for ultrahigh capacity and high-energy density supercapacitors, *ACS Appl. Mater. Interfaces*, 2023, **15**, 36500–36511.

39 D. Yao, F. L. Wang, W. Lei, Y. Hua, X. F. Xia, J. P. Liu and Q. L. Hao, Oxygen vacancies boosting ultra-stability of mesoporous ZnO-CoO@N-doped carbon microspheres for asymmetric supercapacitors, *Sci. China Mater.*, 2020, **63**, 2013–2027.

40 K. Le, M. J. Gao, W. Liu, J. R. Liu, Z. Wang, F. L. Wang, V. Murugadoss, S. D. Wu, T. Ding and Z. H. Guo, MOF-derived hierarchical core-shell hollow iron-cobalt sulfides nanoarrays on Ni foam with enhanced electrochemical properties for high energy density asymmetric supercapacitors, *Electrochim. Acta*, 2019, **323**, 134826.

41 G. Yilmaz, K. M. Yam, C. Zhang, H. J. Fan and G. W. Ho, In situ transformation of MOFs into layered double hydroxide embedded metal sulfides for improved electrocatalytic and supercapacitive performance, *Adv. Mater.*, 2017, **29**, 1606814.

42 X. Q. Zeng, M. Y. Yang, J. Zhao, J. J. Shao and Z. Ding, Iron-doped nickel sulfide nanospheres anchored on reduced graphene oxide for high performance supercapacitors, *Mater. Chem. Front.*, 2024, **8**, 1816–1826.

43 M. J. Yi, C. Q. Zhang, C. Cao, C. Xu, B. S. Sa, D. P. Cai and H. B. Zhan, MOF-derived hybrid hollow submicrospheres of nitrogen-doped carbon-encapsulated bimetallic Ni–Co-S nanoparticles for supercapacitors and lithium ion batteries, *Inorg. Chem.*, 2019, **58**, 3916–3924.

44 S. N. Fu, L. Ma, M. Y. Gan, J. Shen, T. T. Li, X. L. Zhang, W. Zhan, F. Xie and J. Yang, Sn-doped nickel sulfide (Ni_3S_2) derived from bimetallic MOF with ultra high capacitance, *J. Alloys Compd.*, 2021, **859**, 157798.

45 W. Zhao, Y. W. Zheng, L. Cui, D. D. Jia, D. Wei, R. K. Zheng, C. Barrow, W. R. Yang and J. Q. Liu, MOF derived Ni–Co-S nanosheets on electrochemically activated carbon cloth via an etching/ion exchange method for wearable hybrid supercapacitors, *Chem. Eng. J.*, 2019, **371**, 461–469.

46 P. F. Cai, T. Liu, L. Y. Zhang, B. Cheng and J. G. Yu, ZIF-67 derived nickel cobalt sulfide hollow cages for high-performance supercapacitors, *Appl. Surf. Sci.*, 2020, **504**, 144501.

47 D. Wang, L. Y. Tian, J. Y. Huang, D. W. Li, J. Y. Liu, Y. Xu, H. Z. Ke and Q. F. Wei, "One for two" strategy to prepare MOF-derived $NiCo_2S_4$ nanorods grown on carbon cloth for high-performance asymmetric supercapacitors and efficient oxygen evolution reaction, *Electrochim. Acta*, 2020, **334**, 135636.